following any of the previously reported treatments [7]. We next evaluated the regeneration of CST axons using the anterograde tracer biotinylated dextran amine (BDA). We first confirmed sufficient labeling efficiency of BDA tracing in each animal, and no obvious CST regeneration beyond the lesion epicenter was observed in either the control or the semaphorin3A inhibitor treatment group, which is consistent with our previous paper's findings [20] (Figure 3). Moreover, no clear CST regeneration beyond the lesion epicenter was observed in the combined treatment group (Figure 3).

### SM-345431 enhanced angiogenesis and remyelination

Semaphorin3A suppresses VEGF-induced angiogenesis, and inhibition of semaphorin3A leads to enhancement of angiogenesis [29]. This phenomenon occurs because semaphorin3A and VEGF share the same receptor, neuropilin1 [30]. In addition, blood vessels are believed to play important roles in tissue repair and axonal regeneration after SCI [31-33]. Therefore, we analyzed the effects of SM-345431 treatment (using our DDS) on angiogenesis. For immunohistochemistry, we used the anti-RECA-1 antibody, which is known to enable visualization of blood vessels and migrating endothelial cells in rats [32] (Figure 4A). RECA-1-positive areas 3 mm caudal to the lesion epicenter were significantly increased after combined treatment (Figure 4C, $P < 0.05$). Based on their morphology, thick-walled blood vessels with lumen diameters larger than 20 μm are thought to be newly formed blood vessels [34] (Figure 4A,B, arrows). Consistent with previous reports [34,35], these thick-walled blood vessels were rarely observed in the intact spinal cord. In comparison to the control group, the total immunostained areas of vessels with lumen diameters larger than 20 μm were significantly increased in both the SM-345431 and combined treatment groups 3 mm rostral/caudal and 1 mm rostral/caudal to the lesion epicenter (Figure 4D). Furthermore, the effects of angiogenesis tended to be enhanced in the combined treatment group compared to the SM-345431 treatment group, but this difference did not reach statistical significance (Figure 4C,D). Thus, SM-345431 treatment significantly increased the number of newly formed blood vessels.

Semaphorin3A also inhibits oligodendrocyte precursor cell recruitment and influences remyelination [36]. Using immunohistochemistry and electron microscopy, we next characterized the axons at the lesion sites after SM-345431 treatment in greater detail. In the SM-345431 treatment group, we observed substantial numbers of myelinated GAP43-positive axons at the lesion site (Figure 4H-J), whereas myelinated GAP43-positive axons were rarely observed at the lesion site in the control SCT group (Figure 4E-G). Based on their morphologies, the thin

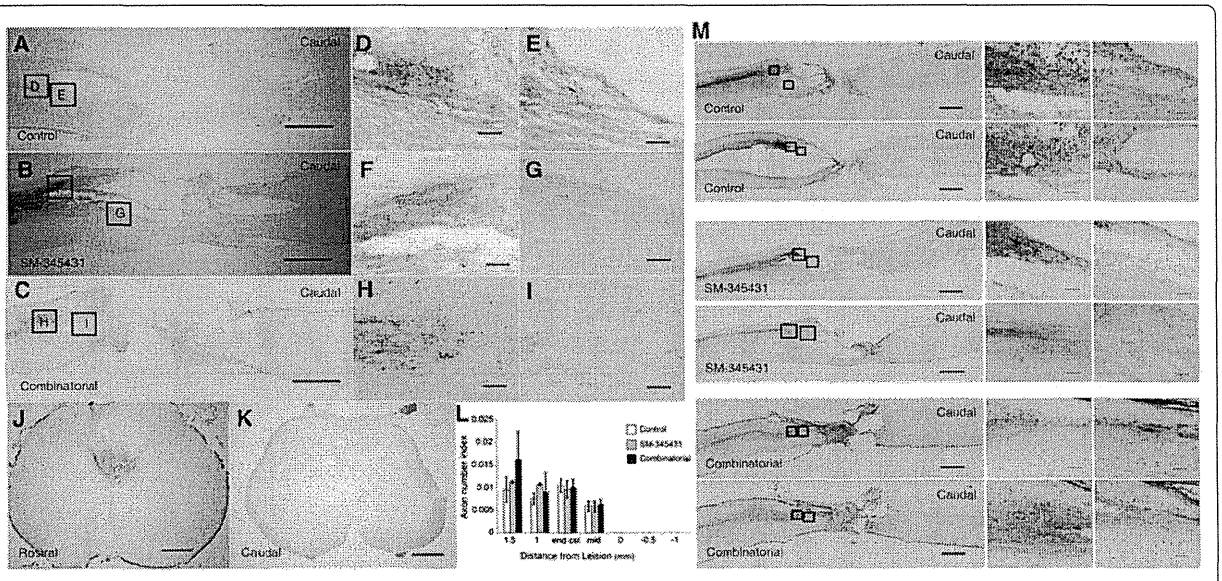


**Figure 3 Histological analyses of the treatment effects on CST regeneration in the injured spinal cord using BDA staining.** **J** shows a representative axial section of the spinal cord at the C4 level (rostral to the lesion site), and **K** shows a representative image of a section at the L4 level (caudal to the lesion site) (Scale bars = 500 μm). Based on these sections, we confirmed that the labeling efficiency of BDA tracing in each animal was sufficient. **A**, **B** and **C** show representative sagittal sections of the BDA staining in each group. **D/E** show magnified images of the boxed area in **A**. Similarly, **F/G** show magnifications of the areas in **B**, and the images in **H/I** are magnifications of the areas in **C**. Scale bars = 1,000 μm in **A-C** and 100 μm in **D-I**. No obvious CST regeneration beyond the lesion epicenter was observed in any of the groups examined **(L)**. Statistical analyses were performed using one-way ANOVA and Bonferroni *post hoc* analyses. Data are presented as the mean ± S.E.M. The images in **M** are representative of other sagittal sections from each group. Scale bars = 1,000 μm in the images on left side of **M** and 100 μm in the magnified images of **M**.

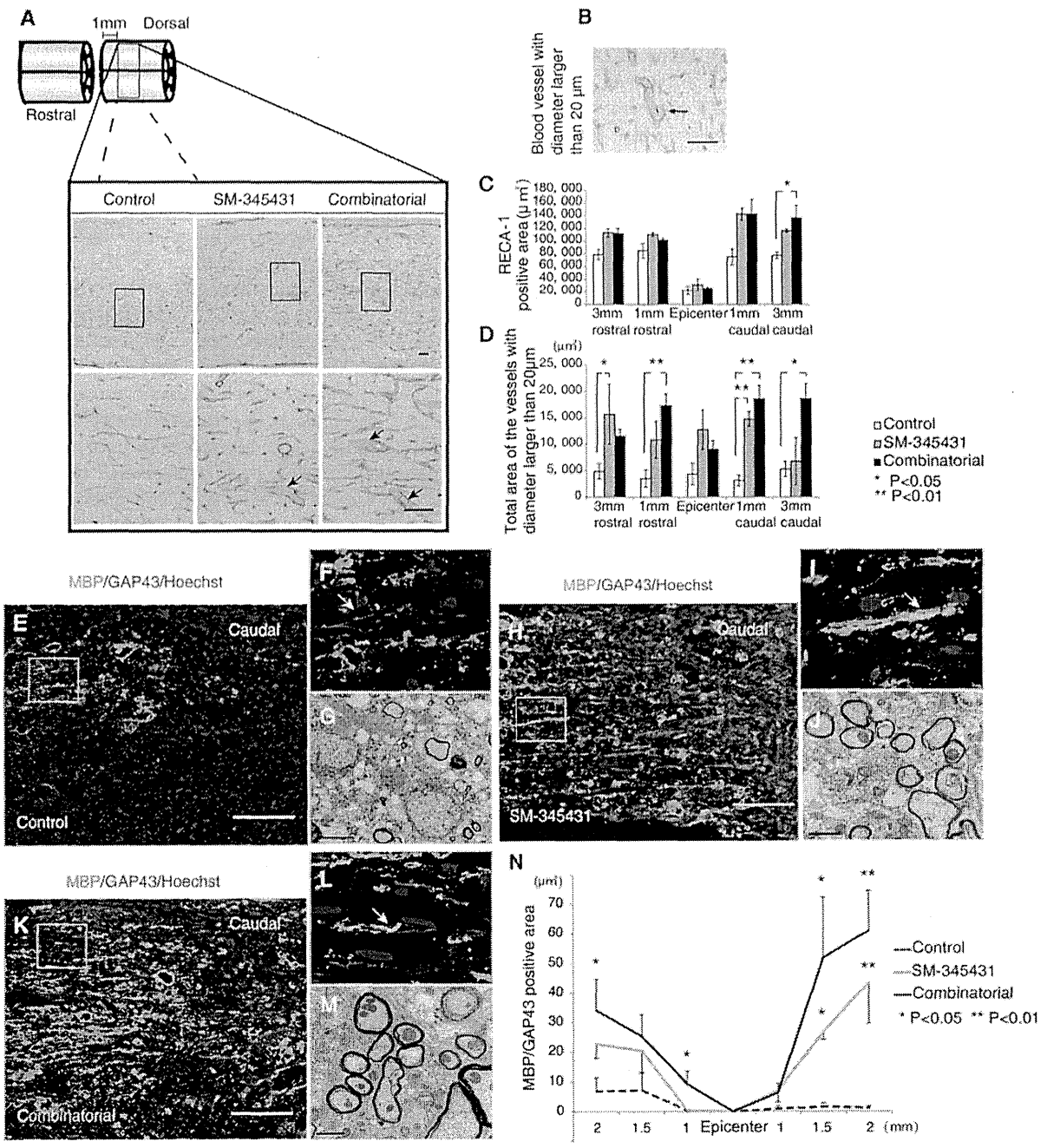


**Figure 4** (See legend on next page.)

(See figure on previous page.)
**Figure 4 Histological analyses of the treatment effects on microvasculature and remyelination in the spinal cord. (A)** Visualization of blood vessels using an anti-RECA-1 antibody. Images in the upper row are low-magnification views of the gray matter areas of sagittal sections immunostained for RECA-1 at 1 mm caudal to the transected site. Scale bars = 50 μm. Images in the lower row are high-magnification views that correspond to the boxed areas in the upper row images. Scale bars = 50 μm. **(B)** Representative image of a blood vessel with a lumen with a diameter larger than 20 μm (arrow), which indicated newly formed blood vessels following injury. Scale bars = 50 μm. Arrows in **(A)** also represent blood vessels with lumen diameters larger than 20 μm. The left side is rostral **(A,B)**. **(C)** Quantitative analysis of RECA-1-positive areas in each group. **(D)** Quantitative analysis of the total areas of RECA-1-positive blood vessels with lumen diameters larger than 20 μm. *P < 0.05, **P < 0.01. Statistical analyses were based on one-way ANOVA and Bonferroni post hoc analyses. **(E-M)** Analyses of remyelination performed using immunohistochemistry against MBP or electron microscopy 12 weeks post-injury. **(E,F,H,I,K,L)** Reconstructed confocal images showing double staining (sagittal sections) for MBP (green) and GAP43 (red) in the control group **(E,F)**, SM-345431 treatment group **(H,I)** and combined group **(K, L)**. **F**, **I** and **L** show magnified images of the boxed areas in **E**, **H** and **K**, respectively. Scale bars = 100 μm. The arrow in **F** shows a non-myelinated (MBP-negative) GAP-43-positive axon, and the arrows in **I** and **L** show myelinated (MBP-positive) GAP-43-positive axons. The left side is rostral. **(G,J)** Electron microscopic images of transverse sections from the control group **(G)** and SM-345431 treatment group **(J)** at the lesion site. Scale bars = 2 μm. **(N)** Statistical analysis of the number of myelinated (MBP-positive) GAP-43-positive axons in each group, which were analyzed by immunohistochemistry. *P < 0.05, **P < 0.01. Statistical analyses were performed using one-way ANOVA and Bonferroni *post hoc* analyses. All the data are represented as the mean ± S.E.M.

myelin sheathes observed in the SM-345431 group were likely the result of remyelination (Figure 4H-J). While SM-345431 treatment significantly enhanced the remyelination of axons (Figure 4N), additional remyelination was not observed in the SM-345431 plus treadmill training combined group (Figure 4K-N).

### Combining SM-345431 with treadmill training reinforced specific spinal locomotor circuitry and synaptic connectivity

Functional locomotor recovery in spinal cord models is critically dependent on supraspinal connections to CPGs [37]. To examine the combined effects of SM-345431 treatment and treadmill training on the reconstruction of spinal cord circuitry at the lumbar level, we performed immunostaining for c-Fos [38] and synapsin-1 [39,40]. c-Fos is widely used as a marker to measure the extent of the supraspinal drive of specific spinal locomotor circuitries because c-Fos expression in neurons normally increases when after the control of spinal locomotor circuitries' circuitry control is lost [41,42]. Consistent with previous studies, c-Fos expression in nuclei (c-Fos + nuclei) was observed in all rats in levels L1-L5 (Figure 5A-C) [43]. In addition, the number of c-Fos + nuclei tended to be lower at the L1-L5 levels in SM-345431-treated SCI rats than in control SCI rats, but this difference did not reach statistical significance (Figure 5B). Interestingly, the combined treatment group showed a statistically significant decrease in the number of c-Fos + nuclei compared to control SCT rats at the L4 and L5 levels (Figure 5B, $P < 0.01$). We also compared the rostral (L1 + L2) and caudal (L4 + L5) segments of the lumbar enlargement to examine the overall effects of combinatorial treatment (Figure 5C). Compared to the intact group (normal rats), control SCT rats showed a significant increase in c-Fos + nuclei counts in the caudal segments of the lumbar enlargement (L4-5), which is consistent with previous reports (Figure 5C, $P < 0.01$) [24]. On the other hand, after combined treatment, the caudal segments of the lumbar enlargement showed significantly decreased c-Fos + nuclei counts (Figure 5C, $P < 0.01$) as compared to control SCT rats. The number of c-Fos + nuclei also tended to be decreased after SM-345431 treatment alone, although this difference was not statistically significant (Figure 5C). Thus, specific spinal locomotor circuitries, especially in the caudal sections of the lumbar enlargement, were considerably reinforced by combined treatment and, to a lesser extent, by SM-345431 treatment alone.

Synapsin-1, a widely used presynaptic marker, has been used to examine activity-dependent synaptic plasticity and synaptic function [39,40]. In comparison to the control and SM-345431 groups, a statistically significant increase in synapsin-1 expression was observed at the lumbar enlargement level (Figure 5E-N) ($P < 0.01$ compared to the control SCT group; $P < 0.05$ compared to the SM-345431 group) in the combined treatment group. No statistically significant difference was observed between the SM-345431 group and the control SCT group ($P > 0.05$). These results indicated that, while SM-345431 treatment alone had a limited effect, SM-345431 treatment combined with treadmill training significantly reinforced synaptic plasticity and function at the lumbar enlargement level.

Taken together, these data suggest that reinforcement of specific spinal locomotor circuitries and motor learning occurred in the lumbosacral circuits of adult rats after combined treatment. These effects were also observed, to a lesser extent, after SM-345431 treatment alone.

### SM-345431 promoted motor functional recovery and combined treatment enhanced this recovery

Next, we investigated the hindlimb motor functions of rats while they walked on a treadmill (induced by a robotic device) using kinematic analysis. In the control SCT rats, hindlimb motor functions showed almost no recovery throughout the period of our experiments (3 months). The SCT rats were unable to take any steps on a treadmill even 3 months post-injury, whereas the treated animals

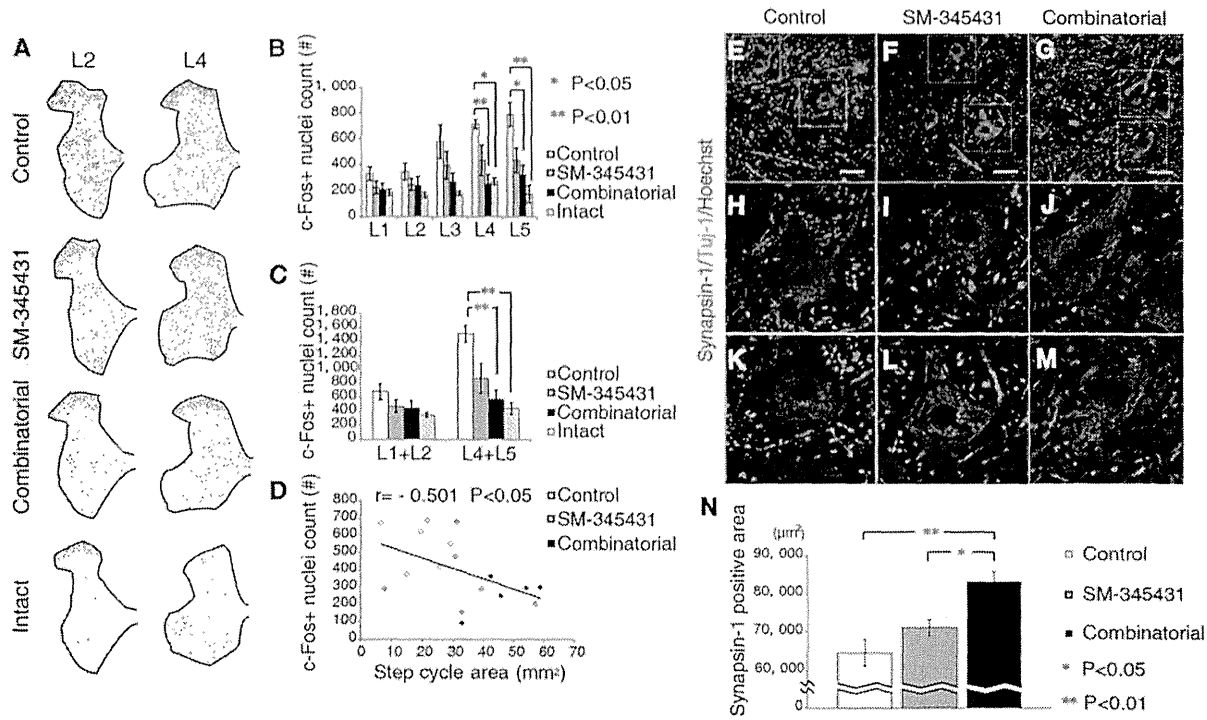


**Figure 5 Immunohistochemical analyses of the effects of treatment on functional remodeling of spinal circuits and synaptic connectivity at the lumbar enlargement. (A)** Representative Camera Lucida drawings of c-Fos + nuclei in transverse sections at the L2 and L4 levels from control rats, SM-345431 treatment rats, combined treatment rats and intact rats. **(B)** Average total numbers of c-Fos + nuclei at each level of the lumbar spinal segment. **(C)** Average total number of c-Fos + nuclei in rostral (L1 + L2) and caudal (L4 + L5) lumbar enlargement segments. **(D)** Correlation analysis between the total number of c-Fos + nuclei in all segments of the lumbar enlargement and step ability on the treadmill. SM-345431 treatment produced a trend toward decreases in the average number of c-Fos + nuclei, although this trend was not statistically significant compared to the control and SM-345431 treatment groups. However, the combined treatment produced a statistically significant decrease in the number of c-Fos + nuclei, suggesting that specific spinal locomotor circuitry was reinforced by combining SM-345431 treatment with extensive treadmill training. *P < 0.05, **P < 0.01. Statistical analyses were performed using one-way ANOVA and Bonferroni post hoc analyses. Data are presented as the mean ± S.E.M. **(E-M)** Representative reconstructed confocal images of double staining (transverse section) for synapsin-1 and Tuj-1 in the ventricolumnar area of the spinal cord (**E-G**: low-magnification images, **H-M**: high-magnification images). **H-J** and **K-M** show the upper and lower boxed areas in **E-G**, respectively. Scale bars = 50 μm. **(N)** Quantitative analysis of synapsin-1 expression in the ventricolumnar motor neuron area 3 months after SCT. *P < 0.05, **P < 0.01. Statistical analyses were performed using one-way ANOVA and Bonferroni *post hoc* analyses. Data are presented as the mean ± S.E.M.

showed some degree of motor function recovery. We performed Bonferroni *post hoc* analyses to examine the differences in step length and step height between the groups (Figure 6A) and found that motor function was significantly better in SM-345431 rats than in control SCT rats (Figure 6B-C). Furthermore, SM-345431 treatment with treadmill training further improved motor performance as compared to no treatment (Figure 6B,C,D,E) or SM-345431 treatment alone (Figure 6D,E). To evaluate motor functions in greater detail, we examined the "step cycle area", which was calculated by multiplying the average step length and average step height as previously described [44] (Figure 6F). This parameter includes elements of both the horizontal and vertical step planes and can thus be regarded as a 2-dimensional evaluation of each step taken. We again performed Bonferroni *post hoc* analyses to statistically compare the differences between the groups. In the SM-345431-treated rats, a statistically significant enhancement of the step cycle area was observed in comparison to the control SCT rats ($P < 0.05$ at 3 months). Furthermore, the combined treatment resulted in an even greater improvement in step cycle area when compared to control SCT rats ($P < 0.05$ at the first month, $P < 0.01$ at the second month, $P < 0.01$ at the third month). As previously described [20], the control SCT rats could not take any steps on the treadmill even at 3 months post-injury (Figure 6G,H and Additional file 1). Without extensive treadmill training, the effects of SM-345431 treatment were moderate and did not result in plantar step walking, even with the BSS (Figure 6G,H and Additional file 1). However, when combined with extensive treadmill training, SM-345431 treatment led

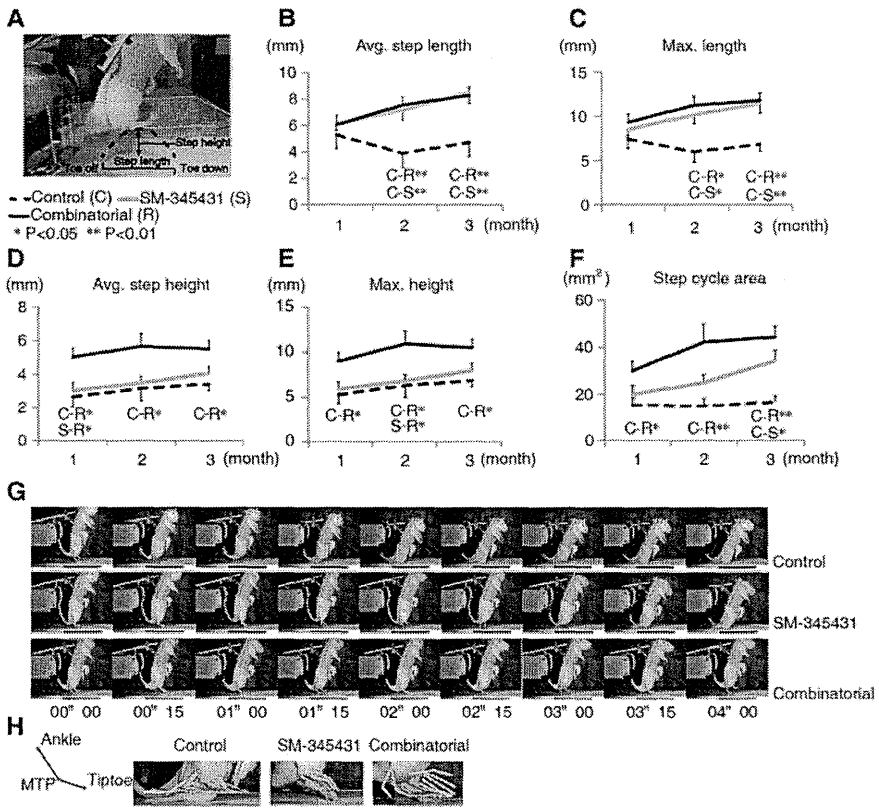


**Figure 6 Detailed kinematic analysis of hindlimb motor performance on the treadmill. (A)** Representative image of the analysis and a schematic diagram of the step parameters. Collected kinematic data from each group showing the average step lengths **(B)**, maximum step lengths **(C)**, average step heights **(D)**, maximum step heights **(E)** and step cycle areas **(F)**. All of these data were recorded and analyzed using a robotic device (Rodent Robot 3000; Robomedica Inc.). Each kinematic analysis was performed at 70% BWS and a speed of 1 cm/s over 1 min. C represents the control group, S represents the SM-345431 group, and R represents the combined treatment group. *P < 0.05, **P < 0.01. C-S* indicates that a statistically significant difference was observed between the control and SM-345431 groups at P < 0.05. Statistical analyses were performed using one-way ANOVA with Bonferroni *post hoc* analyses. Data are presented as the means ± S.E.M. **(G)** Representative sequential pictures of steps taken during the first 4 s of the analysis (BWS: 70%, speed: 3 cm/s). **(H)** Kinematic characteristics of the first step taken in each group. SM-345431 treatment enhanced motor function recovery on the treadmill, especially in terms of the step length parameters. Combined treatment further enhanced the motor function recovery, especially in terms of the step height and step cycle area parameters.

to considerably enhanced motor function recovery; all rats exposed to the combined treatment achieved continuous plantar step walking on a treadmill with the BSS for at least 30 min (Figure 6G,H and Additional file 1).

Specifically, SM-345431 treatment improved locomotor function on a treadmill after SCT particularly in terms of the step length parameters (Figure 6B,C: average and maximum step lengths). Regarding the step height parameter, the effect of SM-345431 treatment was moderate and statistically insignificant (Figure 6D,E). However, when SM-345431 treatment was combined with extensive treadmill training, greater enhancement was observed, and this enhancement extended to the step height parameter (Figure 6D,E; average and maximum step heights). Furthermore, the incremental effects of the treatments over time on motor function performance, specifically on step height and step cycle area, did not reach a plateau by the end of the experimental period (3 months post-injury). At this time, the incremental effects tended to be more robust in the SM-345431 treatment group than in the combined treatment group (Figure 6F: step cycle area). Interestingly, we also discovered a statistically significant correlation between the number of c-Fos + nuclei and motor function (step cycle area) within each group; the c-Fos + nuclei counts were inversely correlated with the extent of functional motor recovery (Figure 5D; r = -0.501, P < 0.05).

We next examined the extent to which the regenerated axons at the lesion sites contributed to motor function recovery in each group. We performed re-transection of the initial lesion site 12 weeks after the initial injury, and we also performed the kinematic analysis before and after the re-transectioning procedure. None of the step parameters changed significantly in the control group, whereas the

step cycle area tended to be attenuated in the SM-345431 group after re-transection (Figure 7). Interestingly, greater attenuations of step ability were observed in all analyzed parameters in the combined treatment group after re-transection, and some of these parameters (step height) were statistically significant (Figure 7, average step height: $P < 0.01$; maximum step height: $P < 0.05$). Thus, the regenerated axons at the lesion site contributed, at least partially, to the enhancement of motor function recovery.

## Discussion

With clinical applications in mind, we first sought to find an appropriate and efficient way to deliver our semaphorin3A inhibitor to transected spinal cords to reestablish useful motor function after SCI. For this purpose, we developed a novel DDS and tested its therapeutic potential *in vivo*. Furthermore, we tested whether specific rehabilitation had the capability to reinforce motor function in the SCT model after treatment with the semaphorin3A inhibitor. Our results can be briefly summarized as follows. First, our newly developed DDS utilizing silicone sheets provided continuous and stable drug delivery and therefore demonstrated potential clinical application. Second, motor function recovery was considerably enhanced by combining SM-345431, the novel semaphorin3A inhibitor, with treadmill training, and this combined treatment enabled paralyzed rats to perform continuous plantar step walking on a treadmill with a BSS.

Osmotic mini pumps have been widely used for drug delivery in animal models of SCI [20,45]. While these pumps are excellent for controlling the drug release dosage and the accurate positioning of drug delivery, this method is too invasive for use in most patients. Therefore, we developed a new silicone matrix preparation as a novel DDS and showed that this novel DDS provided stable and continuous release of SM-345431 throughout the experimental period. In addition, because SM-345431 shows a better stability in a silicone sheet than SM-216289 and approximately the same semaphorin3A inhibitory activity as SM-216289, we used SM-345431 instead of SM-216289 in the present study. As a result, significantly enhanced axonal regeneration and motor function recovery were observed after SM-345431 treatment, which is consistent with our previous study using SM-216289 and osmotic mini pumps [20]. Therefore, this novel DDS demonstrated strong potential for future clinical use.

In this study, we examined the effects of a new semaphorin3A inhibitor, SM-345431, on axonal regeneration and motor function recovery after SCT. Our data indicated that SM-345431 administration using the novel DDS was effective in promoting axonal regeneration and motor function recovery *in vivo*. However, consistent with the results of our previous study using SM-216289, these effects were moderate [20]. More importantly, we found that motor function recovery was significantly enhanced by combining SM-345431 with extensive treadmill training (Figure 6). This combined strategy enabled paralyzed rats to perform continuous plantar step walking on a treadmill with a BSS. Previous work has also demonstrated that intact or injured axons in descending tracts and propriospinal circuits can undergo spontaneous anatomical and physiological remodeling after SCI [46,47] to allow the relay of information through endogenous spinal circuits. Subsequently, the novel propriospinal relay connections bypass the injury epicenter to induce supraspinal control and some degree of motor function recovery. This phenomenon has also been observed following the irreversible interruption of long descending tracts in mice [48]. Because SM-345431 treatment without extensive treadmill training had limited effects on anatomical reconstruction in the lumbar enlargement

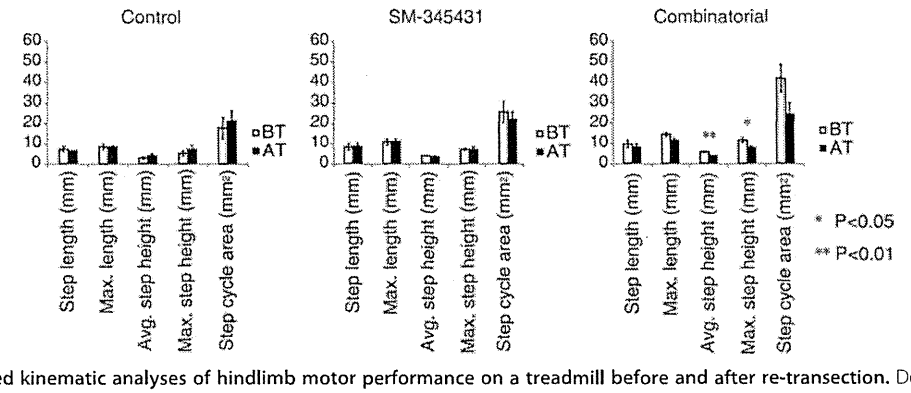


**Figure 7 Detailed kinematic analyses of hindlimb motor performance on a treadmill before and after re-transection.** Detailed kinematic analyses of hindlimb motor performance on a treadmill before and after re-transection were performed and analyzed using a robotic device (Rodent Robot 3000; Robomedica Inc.). BT represents before re-transection; AT represents after re-transection. Although none of the step parameters in the control group showed significant changes, the step cycle area parameters were attenuated in the SM-345431 group after re-transection. Further attenuation of the step ability parameters was observed in the combined treatment group after re-transection. *$P < 0.05$ **$P < 0.01$. Statistical analyses were performed using *t*-test analyses. Data are presented as the mean ± S.E.M.

(Figure 5), we speculate that the enhanced motor function recovery observed after SM-345431 treatment resulted mainly from axon regeneration and limited anatomical reconstruction. Enhanced axonal regeneration possibly led to anatomical and physiological remodeling at the lesion site and improved motor function recovery, which is consistent with our previous findings using SM-216289 administered via osmotic mini pumps [20].

Interestingly, while axonal regeneration was not further enhanced by combining SM-345431 treatment with extensive treadmill training (Figure 2), motor function recovery was significantly enhanced (Figure 6). Previous work demonstrated that limited spontaneous axonal regeneration occurs after SCI and that only some of the new axons are useful for motor function recovery [49]. Thus, axonal regeneration alone may not result in sufficient motor function recovery unless these regenerated axons are appropriately connected. We therefore hypothesized that the regenerated axons induced by semaphorin3A inhibitor treatment may exhibit substantially improved rewiring, in terms of the formation of appropriate connections, following extensive treadmill training. Indeed, motor function recovery was enhanced significantly by combined treatment, as paralyzed rats that received combined treatment were able to perform continuous plantar step walking on a treadmill with a BSS (Figure 6). Re-transectioning experiments further suggested that the regenerated axons at the lesion site and their rewiring contributed to the enhancement in motor function recovery observed in the treatment groups (Figure 7). We also observed that some regenerated axons, such as 5-HT-positive raphespinal tract axons, penetrated into the epicenter of the lesion (Figure 2), and these regenerated axons may have contributed to the reorganization of spinal circuitry at the lesion site and enhanced motor function recovery in the treatment groups [20]. Interestingly, we observed greater attenuation of motor function after re-transection in the combined treatment group (Figure 7). Taken together, these data indicate that the regenerated axons achieved substantial rewiring to the appropriate targets at the lesion site, which was associated with the rehabilitation performed in the combined treatment group [21].

Moreover, the enhanced motor function recovery was only partially attenuated after re-transection in the treatment groups. The results of these re-transection experiments in the treatment groups, especially in the combined treatment group, suggested that other factors, such as reorganization of the lumbar spinal circuitry, also contributed to the enhancement of motor function recovery. We also performed re-transection experiments in animals that only received extensive treadmill training (without SM-345431 treatment), and in these animals, only minimum attenuation of motor performance after re-transection was observed (data not shown). This finding further supports the mechanism proposed above. Taken together, it is possible that specific rehabilitation enhances not only the rewiring of the regenerated axons but also the reorganization of the lumbar spinal circuitry [43]. Furthermore, in the combined treatment group, it is possible that the effect of specific rehabilitation on the reorganization of the lumbar spinal circuitry was the main contributor to the enhancement of motor function recovery in the early stage, while the effect on rewiring of the regenerated axons was the main contributor to the enhancement of motor function recovery during the later stage.

The results of c-Fos immunohistochemistry (Figure 5) showed that extensive treadmill training induced plastic changes at a level caudal to the injured site. Interestingly, step ability on the treadmill was significantly correlated with decreases in the numbers of c-Fos-positive nuclei at a level caudal to the lumbar enlargement (Figure 5D). Therefore, enhanced motor function recovery could be partially the result of anatomical reconstruction of the lumbar spinal cord, which is thought to be the location of CPGs [50]. It is now widely accepted that supraspinal drive of CPGs is required for locomotor function [51] and that the intrinsic plasticity of CPGs allows some spontaneous motor function recovery even in the absence of significant axonal regeneration [24,52]. Therefore, it is possible that axon regeneration moderately enhanced motor function recovery in the SM-345431 treatment group, while rewiring of the regenerated axons and CPG activation was achieved by combining the SM-345431 treatment with treadmill training.

Which segment of the lumbar enlargement is most important for improved walking ability on a treadmill? Reportedly, rhythmic bursts are related to flexor activity at the L2 level and to extensor activity at the L5 level [50]. Treadmill training induces plastic changes in the transmission of group I pathways to extensors that consequently support the recovery of weight-supported motion while standing [53]. The present study showed that combined treatment significantly altered c-Fos expression at the L4 and L5 levels (Figure 5B-C) and improved step height (Figure 6D-E) and continuous plantar step walking on the treadmill with a BSS (Figure 6G and Additional file 1). However, while SM-345431 alone improved step ability, this improvement did not lead to continuous plantar step walking (Figure 6). Therefore, axon regeneration alone might have only limited effects on the spinal cord extensor pool, which could explain the limited motor function recovery of SCT rats after SM-345431 treatment alone. However, the combined treatment may have reestablished the function of the extensor pool by rewiring the regenerated axons and remodeling spinal circuits. As a result, important motor functions, such as continuous plantar step walking (on a treadmill with a BSS), may have been reestablished in SCT adult rats in the combined

treatment group. Thus, combining SM-345431 treatment with specific rehabilitation is a reasonable and promising approach to the treatment of SCI.

Other possible mechanisms underlying motor function recovery could include remyelination and angiogenesis. We noticed that, with increases in afferent sensory input, the step lengths of the SM-345431 groups while walking on the treadmill exhibited a linear and gradual improvement throughout the experimental period. The animals treated with SM-345431 showed enhanced remyelination at the lesion site (Figure 4E-J), which could be relevant to a recent study reporting the effects of semaphorin3A on myelination [36]. In general, myelination significantly increases conduction velocity (sometimes up to 100-fold [54]), which results in increased motor function. Thus, remyelination after SM-345431 treatment may have also partially contributed to the enhancement of motor function recovery on the treadmill. Angiogenesis also plays an important role in reducing secondary damage and enhancing tissue repair after SCI, and the extent of angiogenesis correlates with the extent of axon regeneration after SCI [33]. Angiogenesis was significantly enhanced after SM-345431 treatment alone, although combined treatment did not further enhanced this effect statistically (Figure 4A-D). Therefore, angiogenesis may also have contributed to motor function recovery. Interestingly, at the end of the experimental period (3 months post-injury), the incremental effects of the treatment on motor performance, specifically in terms of step height and step cycle area, tended to be more robust in the SM-345431 treatment group than in the combined treatment group (Figure 6D-F). These data indicate that combined treatment may also have expedited motor function recovery and decreased the overall time needed for recovery.

## Conclusions

Collectively, our data demonstrate that the administration of SM-345431 via a novel DDS utilizing silicone sheets significantly enhanced axonal regeneration, remyelination and angiogenesis, thereby promoting motor function recovery after SCT in adult rats. Additionally, combining SM-345431 with extensive treadmill training resulted in improved motor function recovery that included continuous plantar step walking on a treadmill with a BSS. This comprehensive effect of combined treatment presumably resulted from the reinforcement of spinal networks in the caudal spinal stump and the rewiring/refinement of regenerated axons. Thus, combining semaphorin3A inhibitor treatment with extensive treadmill training has great potential as a new treatment for SCI. In addition, this study highlights the importance of combining treatments that promote axon regeneration with specific and appropriate rehabilitations that promote rewiring for the effective treatment of SCI.

## Methods

### Overall experimental outline

Rats were randomly divided into the following three experimental groups: 1) untrained + placebo, 2) untrained + SM-345431 and 3) trained + SM-345431. SCT was performed, and SM-345431 or placebo was administered at the lesion site via the newly developed DDS, which is described in detail below. Starting 1 week post-injury, treadmill training commenced with a BSS. Kinematic tests were performed monthly for 3 months after SCT using a rodent robotic device (Rodent robot 3000, Robomedica Inc.) that primarily assessed the performance of plantar stepping on a treadmill. Treadmill training was continued throughout the experimental period.

### Animals and surgical procedures

A total of 53 adult female Sprague-Dawley rats (200-250 g, 10-12 weeks old) were used in this study (3 rats died during the experimental period and were excluded from the statistical analysis). All procedures were approved by the experimental animal care committee of Keio University, School of Medicine and Murayama Medical Center (approval #12-8). All rats were anesthetized with an intraperitoneal injection of ketamine (100 mg/kg)/xylazine (10 mg/kg). The spinal cord at the level of the T10 lamina was exposed by T10 laminectomy, and the dorsal dura mater was opened. The exposed spinal cord was cut along the inner edge of the vertebra with a sharp micro-scissor. Two more cuts were made at the gap of the transected spinal cord by a scalpel to ensure total transection. SM-345431 or placebo was administered to the transected site via the newly developed DDS as described in detail below (Figure 1G-I). After these procedures, the back muscles and skin were closed. Rats were kept warm in an incubator (37°C) after surgery. To prevent dehydration in the rats, 10 ml of saline was subcutaneously injected daily until day 7. Ampicillin (0.4 g/kg) was also injected intramuscularly daily to prevent infection until day 7. The bladder was evacuated manually until autonomous emptying of the bladder was achieved. The re-transection procedure was performed at the same level as the primary SCT (15 rats total; 5 rats from each group). Kinematic data were recorded using similar procedures prior to re-transection surgery (on the same day) and on the day following re-transection surgery. For CST tracing, 10% BDA was injected as follows. Nine weeks after SM-345431 or placebo administration, BDA (10000 MW, Molecular Probes) was injected into six different sites of the sensorimotor cortices of the rats under general anesthesia (site 1: 2.0 mm lateral, 0 mm to bregma; site 2: 2.0 mm lateral, 2 mm posterior to bregma; site 3: 2.0 mm lateral, 4 mm posterior to bregma; site 4: 4 mm lateral, 0 mm to bregma; site 5: 4 mm lateral, 2 mm posterior to bregma and site 6: 4 mm lateral, 4 mm posterior to bregma). For

each site, injections were performed at two different depths (1.2 mm and 1.6 mm), and 3 μl of 10% BDA was injected at a rate of 0.15 μl/min using a micro-injector. Three weeks after the BDA injection, rats were sacrificed and used for immunohistochemistry.

### Growth cone collapse assay and collagen co-culture assay

The growth cone collapse assay and collagen co-culture experiments were performed as previously described [20]. To examine the effects of SM-345431-silicone, small pieces (2 × 1 × 0.3 mm; approximately 1 mg containing 1 μg of SM-345431) of the SM-345431-silicone or control-silicone were placed in a collagen gel adjacent to E8 chick DRGs and COS7 cell aggregates, as shown in Figure 1C.

### Drug delivery system

A novel matrix silicone preparation was developed to allow continuous drug delivery at the site of injury. The amount of drug released from this matrix silicone preparation *in vitro* was measured as described in Figure 1. Matrix silicone sheets (0.3 mm thick) containing SM-345431 were trimmed into 3-mm-square pieces to fit into the opened dura. After SCT, one piece of silicone sheet was placed on the transected spinal cord gap so that it could act on the spinal cord directly. Silicone sheets of the same size that did not contain SM-345431were used for the control group.

### Training protocol

A robotic device (rodent robot 3000, Robomedica Inc.) [55] was used to train the SCT rats. Briefly, the device consisted of a computer-controlled BSS, two lightweight robotic arms and a treadmill with variable motorized speeds. The ankles of the hindlimbs of rats were held with a pair of releasable rope cuffs, which were then secured to robotic arms to track ankle trajectory in the horizontal and vertical directions. A computer-controlled body support arm was used to control the load that was applied to the hindlimbs and to maintain body equilibrium. Rats were secured in a cloth vest and attached to the body support arm with a hook-and-loop fabric. Hard rope cuffs were attached to the hindlimbs of rats with the robotic arm during training.

In our pilot study, we found that it was possible to train spinal cord-transected rats soon after SCT via voluntary walking evoked by sensory input. Additionally, improvements in motor performance were more obvious when the treadmill training was initiated at earlier time points after SCT. Therefore, training was initiated as early as 1 week after SCT. The fixed parameters were set at 50% body weight support (BWS), 20 min/day and 5 days/week. The animals were adapted to the training via increasing velocity; a velocity of 1 cm/s was used in the first week, and then the velocity was increased by 2 cm/s every 2 weeks for the first 2 months after injury (i.e., 1 cm/s to 3 cm/s to 5 cm/s). In the first week of training, rats frequently did not adapt to the acceleration of the treadmill, and this resulted in dragging of the hindlimbs. Once the rats dragged their hindlimbs and stopped walking on the treadmill, a trainer brought their bodies back to the original walking position. The step ability of SCT rats on the treadmill improved gradually over the course of the first 2 months following injury. However, this improvement was attenuated at time points later than 2 months after injury. Hence, at the time points later than 2 months after injury, the velocities of the treadmill were adjusted to 5 to 9 cm/s according to the improvement observed in the hindlimb motion of the rats.

### Detailed motor function analysis using kinematics

To evaluate the locomotor capability of SCT rats in detail, the aforementioned robotic device was employed. Each robotic arm tracked the two-dimensional movement of the ankle, and the trajectory of the ankle movement was then recorded on a computer for kinematic analyses. Not all the rats were able to walk by themselves on the treadmill by the last time point of the experiment. Therefore, when performing the tests, the degree of BWS and treadmill speed were titrated to obtain the maximum walking performance on the treadmill. As a result of this titration, the behavioral tests were performed at 70% BWS and a treadmill velocity of 1 cm/s each month after SCT. The duration of testing was 1 min per rat to minimize training effects during testing. The methods of previous reports [44,56] were followed with slight adaptations. Briefly, the ankle trajectory in each plane was recorded by the robotic arm and a computer. Then, the toe off (TO) and paw contact (PC) events in each step cycle were identified using Rodent Robot 3000 software. All kinematic characteristics were obtained when TO and PC were identified; as a result, parameters such as the duration phase, the swing phase of the step cycle and the length and height of the step were calculated. The number of animals used in these behavioral tests was 32 (control: n = 9, SM-345431: n = 12, combined: n = 11).

### Immunohistochemistry

Twelve weeks after SCT, rats were deeply anaesthetized by an intraperitoneal injection of 14% chloral hydrate and then perfused intracardially with 4% paraformaldehyde (PFA) in 0.1 M phosphate-buffered saline (PBS). The spinal cord tissues were dissected and post-fixed in 4% PFA (24 h) and placed in 10% sucrose in 0.1 M PBS (24 h) followed by 30% sucrose in 0.1 M PBS (24 h). All the rats other than 3 rats died during the experimental period were used for the histological analysis. Segments of spinal cords were embedded in Optimal Cutting Temperature compound (Tissue Tek) and stored at -80°C. Frozen spinal

cord tissues were cut with a cryostat into 20-μm-thick sections. For diaminobenzidine (DAB) staining, sections were washed with 0.1 M PBS and then presoaked for 30 min in 0.03% $H_2O_2$ with methanol. After an additional presoak in TNB (0.10 M Tris-HCl, 0.15 M NaCl, 0.5% BMP) for 60 min, sections were incubated at 4°C with rabbit anti-GAP43 (1:300; Millipore), mouse anti-rat RECA-1 (1:500; Serotec) or rabbit polyclonal anti-synapsin-1 (1:300; Chemicon) for 24 h. Subsequently, the sections were washed in 0.1 M PBS and incubated with biotinylated secondary antibodies (1:1,000; Jackson Immunoresearch) for 1 h. Next, the sections were washed and then incubated with an avidin-biotin complex (ABC) (Vectastain Elite ABC Kit, Vector Laboratories) in TNB (1:100) and visualized using DAB (Sigma). Sections were rinsed in PBS, dehydrated using ethanol and xylene and cover-slipped with permount. To identify 5-HT-positive axons that penetrated into the scar tissue area after the treatment, we used a previously described double-staining method [28]. 5-HT was visualized using goat anti-serotonin (5-HT) antibody (1:500; ImmunoStar) and DAB with nickel-glucose oxidase, which produced a black stain. Sections were washed and then incubated with rabbit monoclonal anti-glial fibrillary acidic protein (GFAP; 1:1,000; BD Bioscience Pharmingen) and visualized with DAB, which produced a brown stain. Following these procedures, we identified the range of the scars and quantified the number of 5-HT-positive axons that penetrated into the scar tissue area. To evaluate the status of axonal myelination, immunofluorescent double staining was performed using rabbit anti-GAP43 (1:1,000; Millipore) and rat monoclonal anti-MBP (1:50; Abcam) antibodies. Immunohistochemical analysis for c-Fos in spinal neurons was performed using procedures similar to those previously described [24,41,43]. Briefly, rats were trained using the aforementioned training method of continuous hindlimb bipedal stepping. After 45 min of continuous hindlimb bipedal stepping at 3 cm/s with 50% BWS with a hard nylon rope attachment, rats were allowed a 60-min rest. Subsequently, the rats were anesthetized and perfused intracardially with 4% PFA in PBS. After perfusion, the spinal cords were dissected, post-fixed for 24 h at 4°C and cryoprotected in 30% sucrose in PBS for 3 days. The L1-L5 segments were mounted and frozen, and 20-μm-thick axial sections were cut using a cryostat. All sections were pretreated with 0.03% $H_2O_2$ and methanol for 30 min and then incubated with rabbit polyclonal anti-c-Fos antibody (1:200; Santa Cruz Biotechnology) for 24 h (at 4°C). Subsequently, the sections were washed in 0.1 M PBS and incubated in biotinylated secondary antibody (1:1,000; goat antibody against rabbit; Jackson ImmunoResearch) for 1 h. The remaining procedures were identical to those performed for DAB staining, as described above. All images were obtained using either an Axioskop 2 Plus microscope (Zeiss) for DAB staining or a LSM510 confocal microscope (Zeiss) for immunofluorescent staining.

### Electron microscopic analysis

For electron microscopic analysis, rats from the 3 groups were sampled 72 days after injury. Rats were perfused with 4% PFA in PBS, and the spinal cords were dissected and post-fixed with 2.5% glutaraldehyde overnight at 4°C. After 90 min of fixation with 0.5% osmium tetroxide, the spinal cords were dehydrated with ethanol, acetone and QY1 and then embedded. Ultrathin sections at the epicenter of the lesion sites were prepared at a thickness of 80 nm and stained with uranyl acetate and lead citrate for 15 and 12 min, respectively. The sections were observed with a transmission electron microscope (JEOL model 1230), and images were acquired using Digital Micrograph 3.3 (Gatan Inc.).

### Quantitative immunohistochemistry analyses

Immunohistochemical image analyses were performed for all sections of each animal using microscopy, and quantitative analyses were performed by an examiner who was blind to the identities of the animals. Each value is presented as the average value per section (unless otherwise indicated). The number of animals used for quantitative analysis of each staining set ranged from 15 to 21 (5 to 7 animals per group). To quantify the area of GAP-43-positive axons, 5-HT-positive axons and RECA-1-positive vessels, sagittal sections of the spinal cord at the injury site (approximately 1.2 cm in length) were scanned with a CCD camera (DXC-390; Sony). Pictures of the sagittal sections at 1 mm to 3 mm rostral and 1 mm to 3 mm caudal from the injury epicenter were captured for quantitative analyses. The images were analyzed with a Micro Computer Imaging Device (MCID; Imaging Research Inc.). Threshold values were maintained at constant levels for all analyses. 5-HT axons that penetrated into the scar tissue were counted manually. For image analysis, c-Fos-positive (c-Fos+) nuclei from all sections was superimposed onto Molander's cytoarchitectonic maps of the rat thoracic and lumbosacral cord [57]. The expression of synapsin-1 was examined within lamina IX of the L1-L5 segments of the spinal cord using transverse sections and DAB staining. For the quantification of BDA tracing, we followed the methods reported previously [58,59]. The number of CST-positive axons at each distance from the lesion was divided by the number of CST-positive axons at the level of C1 for standardization.

### Statistical analyses

For statistical analyses, one-way analyses of variance (one-way ANOVA) and Bonferroni *post hoc* tests were primarily employed to determine significance. Significance was determined using P-values, and the data are presented

as the means ± S.E.M. For the analysis of 5-HT immunostaining, data were analyzed with the Kruskal-Wallis H test. Behavioral data after re-transection were analyzed with t-tests.

## Additional file

**Additional file 1: Video Representative movies of the *detailed* kinematic *analysis of hindlimb motor performance* on a treadmill at the end of the experimental period.** Plantar step walking with a BSS was not observed in control group animals (A). Limited plantar step walking with a BSS was observed in SM-345431 treatment group animals (B). Significantly enhanced plantar step walking with a BSS was observed in the combined treatment group animals. All animals in the combined treatment group continued plantar step walking with a BSS for at least 30 min (C).

### Competing interests

H. Okano is a scientific consultant of San Bio, Inc; Eisai Co Ltd; and Daiichi Sankyo Co Ltd.
K. Kikuchi, A. Sano, M. Maeda, A. Kishino and T. Kimura are employed by Dainippon Sumitomo Pharma Co Ltd.

### Authors' contributions

LZ and SK performed the experiments and wrote the manuscript. KK, AS, MM, SS, and MM performed the experiments. SK, AK, YT, ML, TK, HO and MM designed the study. All authors read and approved the final manuscript.

### Acknowledgments

We thank Kiyokazu Iwata, Toshihiro Nagai and Takahiro Kondo for sample preparation and all members of the Okano laboratory for helpful discussions and support.
This work was supported by grants from the Project for the Realization of Regenerative Medicine from the Ministry of Education, Culture, Sports and Technology (MEXT) of Japan and the Research Center Network for the Realization of Regenerative Medicine to H.O. and M.N.; a grant for young investigators from MEXT to S.K.; a grant from the General Insurance Association of Japan to L.Z., S.K. and M.N. and the Funding Program for World-Leading Innovative R&D on Science and Technology (FIRST Program) to H.O.

### Author details

[1]Department of Orthopedic Surgery, Keio University School of Medicine, 35 Shinanomachi, Shinjuku, Tokyo 160-8582, Japan. [2]Department of Physiology, Keio University School of Medicine, 35 Shinanomachi, Shinjuku, Tokyo 160-8582, Japan. [3]Department of Rehabilitation Medicine, Keio University School of Medicine, 35 Shinanomachi, Shinjuku, Tokyo 160-8582, Japan. [4]Department of Orthopedic Surgery, National Hospital Organization, Murayama Medical Center, 2-37-1 Gakuen, Musashimurayama, Tokyo 208-0011, Japan. [5]Dainippon Sumitomo Pharma Co. Ltd., 3-1-98 Kasugade-naka, Konohana-ku, Osaka 554-0022, Japan.

Received: 20 January 2014 Accepted: 12 February 2014
Published: 10 March 2014

### References

1. Afshari FT, Kappagantula S, Fawcett JW: **Extrinsic and intrinsic factors controlling axonal regeneration after spinal cord injury.** *Expert Rev Mol Med* 2009, **11**:1–19.
2. Chierzi S, Ratto GM, Verma P, Fawcett JW: **The ability of axons to regenerate their growth cones depends on axonal type and age, and is regulated by calcium, cAMP and ERK.** *Eur J Neurosci* 2005, **21**(8):2051–2062.
3. Davies SJ, Goucher DR, Doller C, Silver J: **Robust regeneration of adult sensory axons in degenerating white matter of the adult rat spinal cord.** *J Neurosci* 1999, **19**(14):5810–5822.
4. Silver J, Miller JH: **Regeneration beyond the glial scar.** *Nat Rev Neurosci* 2004, **5**(2):146–156.
5. Filbin MT: **Myelin-associated inhibitors of axonal regeneration in the adult mammalian CNS.** *Nat Rev Neurosci* 2003, **4**(9):703–713.
6. GrandPre T, Nakamura F, Vartanian T, Strittmatter SM: **Identification of the Nogo inhibitor of axon regeneration as a Reticulon protein.** *Nature* 2000, **403**(6768):439–444.
7. He Z, Koprivica V: **The nogo signaling pathway for regeneration block.** *Annu Rev Neurosci* 2004, **27**(1:341–368.
8. McKerracher L, David S, Jackson DL, Kottis V, Dunn RJ, Braun PE: **Identification of myelin-associated glycoprotein as a major myelin-derived inhibitor of neurite growth.** *Neuron* 1994, **13**(4):805–811.
9. Wang KC, Koprivica V, Kim JA, *et al*: **Oligodendrocyte-myelin glycoprotein is a Nogo receptor ligand that inhibits neurite outgrowth.** *Nature* 2002, **417**(6892):941–944.
10. Bradbury EJ, Moon LD, Popat RJ, *et al*: **Chondroitinase ABC promotes functional recovery after spinal cord injury.** *Nature* 2002, **416**(6881):636–640.
11. McKeon RJ, Schreiber RC, Rudge JS, Silver J: **Reduction of neurite outgrowth in a model of glial scarring following CNS injury is correlated with the expression of inhibitory molecules on reactive astrocytes.** *J Neurosci* 1991, **11**(11):3398–3411.
12. De Winter F, Holtmaat AJ, Verhaagen J: **Neuropilin and class 3 semaphorins in nervous system regeneration.** *Adv Exp Med Biol* 2002, **515**:115–139.
13. Pasterkamp RJ, Giger RJ, Ruitenberg MJ, *et al*: **Expression of the gene encoding the chemorepellent semaphorin III is induced in the fibroblast component of neural scar tissue formed following injuries of adult but not neonatal CNS.** *Mol Cell Neurosci* 1999, **13**(2):143–166.
14. Hata K, Fujitani M, Yasuda Y, *et al*: **RGMa inhibition promotes axonal growth and recovery after spinal cord injury.** *J Cell Biol* 2006, **173**(1):47–58.
15. Schwab JM, Conrad S, Monnier PP, Julien S, Mueller BK, Schluesener HJ: **Spinal cord injury-induced lesional expression of the repulsive guidance molecule (RGM).** *Eur J Neurosci* 2005, **21**(6):1569–1576.
16. Kim JE, Li S, GrandPre T, Qiu D, Strittmatter SM: **Axon regeneration in young adult mice lacking Nogo-A/B.** *Neuron* 2003, **38**(2):187–199.
17. Simonen M, Pedersen V, Weinmann O, *et al*: **Systemic deletion of the myelin-associated outgrowth inhibitor Nogo-A improves regenerative and plastic responses after spinal cord injury.** *Neuron* 2003, **38**(2):201–211.
18. Taniguchi M, Yuasa S, Fujisawa H, *et al*: **Disruption of semaphorin III/D gene causes severe abnormality in peripheral nerve projection.** *Neuron* 1997, **19**(3):519–530.
19. Kikuchi K, Kishino A, Konishi O, *et al*: **In vitro and in vivo characterization of a novel semaphorin 3A inhibitor, SM-216289 or xanthofulvin.** *J Biol Chem* 2003, **278**(44):42985–42991.
20. Kaneko S, Iwanami A, Nakamura M, *et al*: **A selective Sema3A inhibitor enhances regenerative responses and functional recovery of the injured spinal cord.** *Nat Med* 2006, **12**(12):1380–1389.
21. García-Alías G, Barkhuysen S, Buckle M, Fawcett JW: **Chondroitinase ABC treatment opens a window of opportunity for task-specific rehabilitation.** *Nat Neurosci* 2009, **12**(9):1145–1151.
22. Heng C, de Leon RD: **Treadmill training enhances the recovery of normal stepping patterns in spinal cord contused rats.** *Exp Neurol* 2009, **216**(1):139–147.
23. Winchester P, McColl R, Querry R, *et al*: **Changes in supraspinal activation patterns following robotic locomotor therapy in motor-incomplete spinal cord injury.** *Neurorehabil Neural Repair* 2005, **19**(4):313–324.
24. Courtine G, Gerasimenko Y, van den Brand R, *et al*: **Transformation of nonfunctional spinal circuits into functional states after the loss of brain input.** *Nat Neurosci* 2009, **12**(10):1333–1342.
25. Barbeau H, Rossignol S: **Recovery of locomotion after chronic spinalization in the adult cat.** *Brain Res* 1987, **412**(1):84–95.
26. Kubasak MD, Hedlund E, Roy RR, Carpenter EM, Edgerton VR, Phelps PE: **L1 CAM expression is increased surrounding the lesion site in rats with complete spinal cord transection as neonates.** *Exp Neurol* 2005, **194**(2):363–375.
27. Ichiyama R, Gerasimenko Y, Zhong H, Roy R, Edgerton V: **Hindlimb stepping movements in complete spinal rats induced by epidural spinal cord stimulation.** *Neurosci Lett* 2005, **383**(3):339–344.
28. Kubasak MD, Jindrich DL, Zhong H, *et al*: **OEG implantation and step training enhance hindlimb-stepping ability in adult spinal transected rats.** *Brain* 2007, **131**(1):264–276.
29. Acevedo LM, Barillas S, Weis SM, Gothert JR, Cheresh DA: **Semaphorin 3A suppresses VEGF-mediated angiogenesis yet acts as a vascular permeability factor.** *Blood* 2008, **111**(5):2674–2680.

30. Kolodkin AL, VD L, *et al*: neuropilin is a semaphorin III receptor. *Cell* 1997, **90**:753–762.
31. Guizarsahagun G, Ibarra A, Espitia A, Martinez A, Madrazo I, Francobourland R: Glutathione monoethyl ester improves functional recovery, enhances neuron survival, and stabilizes spinal cord blood flow after spinal cord injury in rats. *Neuroscience* 2005, **130**(3):639–649.
32. Imperato-Kalmar EL, McKinney RA, Schnell L, Rubin BP, Schwab ME: Local changes in vascular architecture following partial spinal cord lesion in the rat. *Exp Neurol* 1997, **145**(2 Pt 1):322–328.
33. Loy DN, Crawford CH, Darnall JB, Burke DA, Onifer SM, Whittemore SR: Temporal progression of angiogenesis and basal lamina deposition after contusive spinal cord injury in the adult rat. *J Comp Neurol* 2002, **445**(4):308–324.
34. Casella GTB, Marcillo A, Bunge MB, Wood PM: New vascular tissue rapidly replaces neural parenchyma and vessels destroyed by a contusion injury to the Rat spinal cord. *Exp Neurol* 2002, **173**(1):63–76.
35. Kitamura K, Iwanami A, Nakamura M, *et al*: Hepatocyte growth factor promotes endogenous repair and functional recovery after spinal cord injury. *J Neurosci Res* 2007, **85**(11):2332–2342.
36. Piaton G, Aigrot MS, Williams A, *et al*: Class 3 semaphorins influence oligodendrocyte precursor recruitment and remyelination in adult central nervous system. *Brain* 2011, **134**(4):1156–1167.
37. Kiehn O: Locomotor circuits in the mammalian spinal cord. *Annu Rev Neurosci* 2006, **29**:279–306.
38. Kiehn O, Kjaerulff O: Distribution of central pattern generators for rhythmic motor outputs in the spinal cord of limbed vertebrates. *Ann N Y Acad Sci* 1998, **860**:110–129.
39. Gulino R, Dimartino M, Casabona A, Lombardo SA, Perciavalle V: Synaptic plasticity modulates the spontaneous recovery of locomotion after spinal cord hemisection. *Neurosci Res* 2007, **57**(1):148–156.
40. Ying Z, Roy R, Edgerton V, Gomezpinilla F: Exercise restores levels of neurotrophins and synaptic plasticity following spinal cord injury. *Exp Neurol* 2005, **193**(2):411–419.
41. Ahn SN, Guu JJ, Tobin AJ, Edgerton VR, Tillakaratne NJ: Use of c-fos to identify activity-dependent spinal neurons after stepping in intact adult rats. *Spinal Cord* 2006, **44**(9):547–559.
42. Huang A, Noga B, Carr P, Fedirchuk B, Jordan L: Spinal cholinergic neurons activated during locomotion: localization and electrophysiological characterization. *J Neurophysiol* 2000, **83**:3537–3547.
43. Ichiyama RM, Courtine G, Gerasimenko YP, *et al*: Step training reinforces specific spinal locomotor circuitry in adult spinal rats. *J Neurosci* 2008, **28**(29):7370–7375.
44. de Leon RD, Acosta CN: Effect of robotic-assisted treadmill training and chronic quipazine treatment on hindlimb stepping in spinally transected rats. *J Neurotrauma* 2006, **23**(7):1147–1163.
45. Maier IC, Ichiyama RM, Courtine G, *et al*: Differential effects of anti-Nogo-A antibody treatment and treadmill training in rats with incomplete spinal cord injury. *Brain* 2009, **132**(6):1426–1440.
46. Bareyre FM, Kerschensteiner M, Raineteau O, Mettenleiter TC, Weinmann O, Schwab ME: The injured spinal cord spontaneously forms a new intraspinal circuit in adult rats. *Nat Neurosci* 2004, **7**(3):269–277.
47. Raineteau O, Schwab ME: Plasticity of motor systems after incomplete spinal cord injury. *Nat Rev Neurosci* 2001, **2**:263–273.
48. Courtine G, Song B, Roy RR, *et al*: Recovery of supraspinal control of stepping via indirect propriospinal relay connections after spinal cord injury. *Nat Med* 2008, **14**(1):69–74.
49. Dunlop SA: Activity-dependent plasticity: implications for recovery after spinal cord injury. *Trends Neurosci* 2008, **31**(8):410–418.
50. Kiehn O, Kjaerulff O: Spatiotemporal characteristics of 5-HT and dopamine-induced rhythmic hindlimb activity in the in vitro neonatal rat. *J Neurophysiol* 1996, **75**(4):1472–1482.
51. Feraboli-Lohnherr D, Orsal D, Yakovleff A, Gimenez y Ribotta M, Privat A: Recovery of locomotor activity in the adult chronic spinal rat after sublesional transplantation of embryonic nervous cells: specific role of serotonergic neurons. *Exp Brain Res* 1997, **113**(3):443–454.
52. Edgerton VR, Tillakaratne NJK, Bigbee AJ, de Leon RD, Roy RR: Plasticity of the spinal neural circuitry after injury. *Annu Rev Neurosci* 2004, **27**(1):145–167.
53. Cote MP, Menard A, Gossard JP: Spinal cats on the treadmill: changes in load pathways. *J Neurosci* 2003, **23**(7):2789–2796.
54. Nave K-A: Myelination and support of axonal integrity by glia. *Nature* 2010, **468**(7321):244–252.
55. Nessler JA, Timoszyk W, Merlo M, *et al*: A robotic device for studying rodent locomotion after spinal cord injury. *IEEE Trans Neural Syst Rehabil Eng* 2005, **13**(4):497–506.
56. Timoszyk W, Nessler J, Acosta C, *et al*: Hindlimb loading determines stepping quantity and quality following spinal cord transection. *Brain Res* 2005, **1050**(1–2):180–189.
57. Molander C, Xu Q, Grant G: The cytoarchitectonic organization of the spinal cord in the rat. I. The lower thoracic and lumbosacral cord. *J Comp Neurol* 1984, **230**(1):133–141.
58. Wang D, Ichiyama RM, Zhao R, Andrews MR, Fawcett JW: Chondroitinase combined with rehabilitation promotes recovery of forelimb function in rats with chronic spinal cord injury. *J Neurosci* 2011, **31**(25):9332–9344.
59. Zheng B, Ho C, Li S, Keirstead H, Steward O, Tessier-Lavigne M: Lack of enhanced spinal regeneration in Nogo-deficient mice. *Neuron* 2003, **38**(2):213–224.

doi:10.1186/1756-6606-7-14
**Cite this article as:** Zhang *et al.*: Rewiring of regenerated axons by combining treadmill training with semaphorin3A inhibition. *Molecular Brain* 2014 **7**:14.

Takano et al. Journal of Neuroinflammation 2014, 11:40
http://www.jneuroinflammation.com/content/11/1/40

JNI JOURNAL OF NEUROINFLAMMATION

RESEARCH Open Access

# Inflammatory cascades mediate synapse elimination in spinal cord compression

Morito Takano[1,2], Soya Kawabata[1,2], Yuji Komaki[2,3], Shinsuke Shibata[2], Keigo Hikishima[2,3], Yoshiaki Toyama[1], Hideyuki Okano[2*] and Masaya Nakamura[1*]

## Abstract

**Background:** Cervical compressive myelopathy (CCM) is caused by chronic spinal cord compression due to spondylosis, a degenerative disc disease, and ossification of the ligaments. Tip-toe walking Yoshimura (*twy*) mice are reported to be an ideal animal model for CCM-related neuronal dysfunction, because they develop spontaneous spinal cord compression without any artificial manipulation. Previous histological studies showed that neurons are lost due to apoptosis in CCM, but the mechanism underlying this neurodegeneration was not fully elucidated. The purpose of this study was to investigate the pathophysiology of CCM by evaluating the global gene expression of the compressed spinal cord and comparing the transcriptome analysis with the physical and histological findings in *twy* mice.

**Methods:** Twenty-week-old *twy* mice were divided into two groups according to the magnetic resonance imaging (MRI) findings: a severe compression (S) group and a mild compression (M) group. The transcriptome was analyzed by microarray and RT-PCR. The cellular pathophysiology was examined by immunohistological analysis and immuno-electron microscopy. Motor function was assessed by Rotarod treadmill latency and stride-length tests.

**Results:** Severe cervical calcification caused spinal canal stenosis and low functional capacity in *twy* mice. The microarray analysis revealed 215 genes that showed significantly different expression levels between the S and the M groups. Pathway analysis revealed that genes expressed at higher levels in the S group were enriched for terms related to the regulation of inflammation in the compressed spinal cord. M1 macrophage-dominant inflammation was present in the S group, and cysteine-rich protein 61 (Cyr61), an inducer of M1 macrophages, was markedly upregulated in these spinal cords. Furthermore, C1q, which initiates the classical complement cascade, was more upregulated in the S group than in the M group. The confocal and electron microscopy observations indicated that classically activated microglia/macrophages had migrated to the compressed spinal cord and eliminated synaptic terminals.

**Conclusions:** We revealed the detailed pathophysiology of the inflammatory response in an animal model of chronic spinal cord compression. Our findings suggest that complement-mediated synapse elimination is a central mechanism underlying the neurodegeneration in CCM.

**Keywords:** cervical compressive myelopathy, tip-toe walking Yoshimura mice, complement activation classical pathway, synapse elimination

* Correspondence: hidokano@a2.keio.jp; masa@a8.keio.jp
[2]Department of Physiology, Keio University School of Medicine, 35 Shinanomachi, Shinjuku-ku, Tokyo 160-8582, Japan
[1]Department of Orthopedic Surgery, Keio University School of Medicine, 35 Shinanomachi, Shinjuku-ku, Tokyo 160-8582, Japan
Full list of author information is available at the end of the article

## Background

Cervical compressive myelopathy (CCM) is caused by chronic spinal cord compression due to spondylosis, a degenerative disease of the cervical discs, and ossification of the posterior longitudinal ligaments or yellow ligaments [1,2]. The symptoms appear mainly in the elderly, and include slowly progressive clumsiness and paresthesia in the hands, gait disturbance, and tetraplegia. Human histological studies revealed degeneration of the anterior horns, cavity formation, and demyelination in the severely compressed spinal cord [3,4]. Reports on the surgical outcomes of these patients demonstrate that increased spinal cord stenosis is associated with a worse postoperative recovery [5,6]. Although severe spinal cord compression is known to cause irreversible neurological damage, it is unclear how these pathological changes occur.

Tip-toe walking Yoshimura (*twy*) mice, which develop progressive spinal cord dysfunction secondary to extradural calcified deposits at the C2/3 ligaments, are reported to be a good in vivo model for the pathological changes related to CCM [7-9]. Because this mouse develops spinal cord compression spontaneously, there are individual differences in the severity of spinal cord compression [10]. Previous histological studies have shown that neurons are lost due to apoptosis in *twy* mice [11-13], but the exact mechanism of the neurodegeneration has not been fully elucidated. The purpose of this study was to investigate the pathophysiology of CCM by evaluating the global gene expression of the compressed spinal cord and comparing the transcriptome analysis with physical and histological findings in *twy* mice.

## Methods

### Animal model

The *twy* mice were obtained from a breeding colony of the Central Institute for Experimental Animals (Kawasaki, Japan). The mutant *twy* mice were maintained by brother-sister matings of heterozygotes at the Central Research Institute [11,14]. The *twy* mice harbor an autosomal recessive mutation in the nucleotide pyrophosphatase (*NPPS*) gene [7]. The mice were housed in groups under a 12-hour light/dark cycle, with access to food and water ad libitum. All experiments were performed in accordance with the Guidelines for the Care and Use of Laboratory Animals of Keio University School of Medicine and the Central Institute for Experimental Animals.

### Magnetic resonance imaging

Magnetic resonance imaging (MRI) was performed on the mice at 6, 15, and 20 weeks of age using a 7.0-Tesla magnet (BioSpec 70/16; Bruker BioSpin, Ettlingen, Germany) with a cryogenic quadrature RF surface probe (CryoProbe; Bruker BioSpin AG, Fällanden, Switzerland) to improve the sensitivity [15-18]. The MRI was performed under general anesthesia induced by the intramuscular injection of ketamine (50 mg/kg; Sankyo, Tokyo, Japan) and xylazine (5 mg/kg; Bayer, Leverkusen, Germany) and maintained by isoflurane (Foren; Abbott, Tokyo, Japan). The animal's pulse, arterial oxygen saturation, and rectal temperature were monitored during the MRI. The scanning parameters were as follows: Saggital T2-weighted images (RARE, eTE/TR: 37.5/2000 ms), axial T2-weighted images (RARE, eTE/TR: 21.5 ms/1200 ms). To examine the extent of spinal cord compression due to extradural calcified deposits, the transverse areas of the calcification and spinal canal were measured on the axial T2-weighted images of the *twy* mice, and the canal stenosis ratio was calculated as reported previously [10].

### Behavioral analyses

The motor function of 20-week-old *twy* mice was evaluated using a Rotarod treadmill apparatus (Muromachi Kikai Co., Ltd., Tokyo, Japan) and the DigiGait Image Analysis System (Mouse Specifiics, Quincy, MA, USA). In the Rotarod treadmill test, the time (latency) that each mouse spent on the rod as it rotated at 10 rpm in a 2-min session, was monitored [19]. Three trials were conducted, and the average number of seconds was recorded. In the footprint analysis using the Digigait system, the stride length of the fore and hindlimb was measured as long as the *twy* mouse could walk with consistent weight-supported forelimb steps, on a treadmill set at a speed of 8 cm/s.

### Gene expression analysis

After the in vivo MRI analysis, the *twy* mice were anesthetized and transcardially perfused with heparinized saline (5 U/ml). Dissected segments of the cervical spinal cords were rapidly frozen and placed in TRIzol (Invitrogen, CA, USA). The total RNA was isolated using an RNeasy Mini Kit (Qiagen, Hilgen, Germany) according to the manufacturer's instructions. For the microarray analysis, Cyanine-3 (Cy3)-labeled cRNA was prepared from 100 ng of RNA using the One-Color Low RNA Input Liner Amplification kit (Agilent, CA, USA), followed by RNAeasy column purification (Qiagen). Cy3-labeled cRNA (1.5 μg) was fragmented at 60°C for 30 minutes in a reaction volume of 50 μl containing the Fragmentation Buffer and Blocking Agent included in the kit (Agilent). On completion of the fragmentation reaction, 50 μl of the HI-RPM Hybridization Buffer (Agilent) was added to the fragmentation mixture, and the samples were hybridized to Agilent SurePrint G3 Mouse GE 8 × 60 K Microarrays (G4852A, Agilent) for 17 hours at 65°C in a rotating Agilent hybridization oven. After hybridization, the microarrays were washed for 1 minute at room temperature with GE Wash Buffer 1 (Agilent) and for 1 minute with 37°C GE Wash Buffer 2 (Agilent),

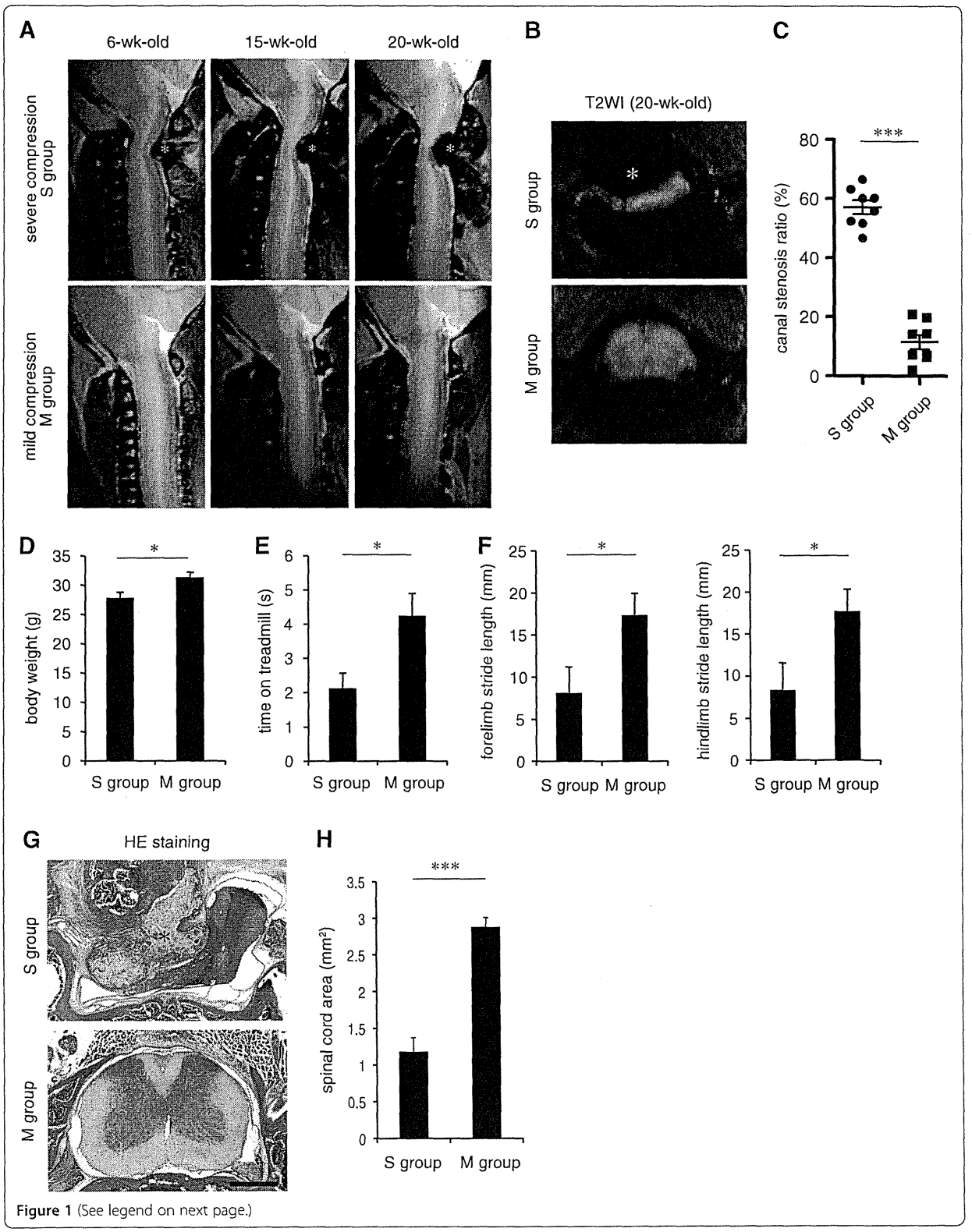


**Figure 1** (See legend on next page.)

(See figure on previous page.)
**Figure 1 Physical and histological differences between severely and mildly compressed spinal cord in tip-toe walking Yoshimura *(twy)* mice. (A)** Representative sagittal T2-weighted images of the severely compressed (S group) and mildly compressed (M group) spinal cords in *twy* mice (6, 15, and 20 weeks of age). **(B)** Representative axial T2-weighted images of the S and M groups at 20 weeks of age. Magnetic resonance imaging (MRI) of the S group **(A, B)** showed clear cervical spinal cord compression resulting from C2/3 ligamentous calcification (*). **(C)** The canal stenosis ratio of the S group was significantly higher than that of the M group ($n = 8$ mice per group). ***$P < 0.001$. **(D)** Body weight in each group ($n = 8$ mice per group). *$P < 0.05$. **(E, F)** Motor functional analyses: Latency on the rotating rod and stride length in each group ($n = 8$ mice per group). *$P < 0.05$. **(G)** Representative HE-stained axial images of the S and M groups in *twy* mice. Scale bar: 500 μm. **(H)** Quantitative analysis of the spinal cord area in the S and M groups ($n = 4$ mice per group). ***$P < 0.001$.

then dried immediately by a brief centrifugation. Immediately after being washed, the slides were scanned on a DNA Microarray Scanner (G2565CA, Agilent) using the one color scan setting for 8 × 60 K array slides. The scanned images were analyzed with the Feature Extraction Software v10.7.3.1 (Agilent) using default parameters to obtain background-subtracted and spatially detrended Processed Signal intensities.

For the clustering analysis, the normalized data were narrowed down by the cut-off values of each expression signal (>50) and fold change (>1.5, for the signal of severely compressed spinal cords versus the signal of mildly compressed spinal cords). The heat map was visualized by Gene Spring GX12 (Agilent). Pathway enrichment analysis was performed for the genes that showed differences on the microarray. RT-PCR was performed on an ABI 7900HT (Applied Biosystems, CA, USA) with TaqMan probes (Applied Biosystems).

### Histological analysis

*Twy* mice were anesthetized and transcardially perfused with 4% paraformaldehyde in 0.1 M PBS. The spinal cord and spinal canal were removed and immersed in Decalcifying Solution B (Dako, Glostrup, Denmark) for three days. These samples were then embedded in OCT compound (Sakura Finetechnical Co., Ltd., Tokyo, Japan) and sectioned in the axial plane at 20 μm on a cryostat (Leica CM3050 S, Wetzlar, Germany). The spinal cords and spinal canals were histologically evaluated by Hematoxylin-eosin (HE) staining and immunohistochemistry. The tissue sections were stained with the following primary antibodies:

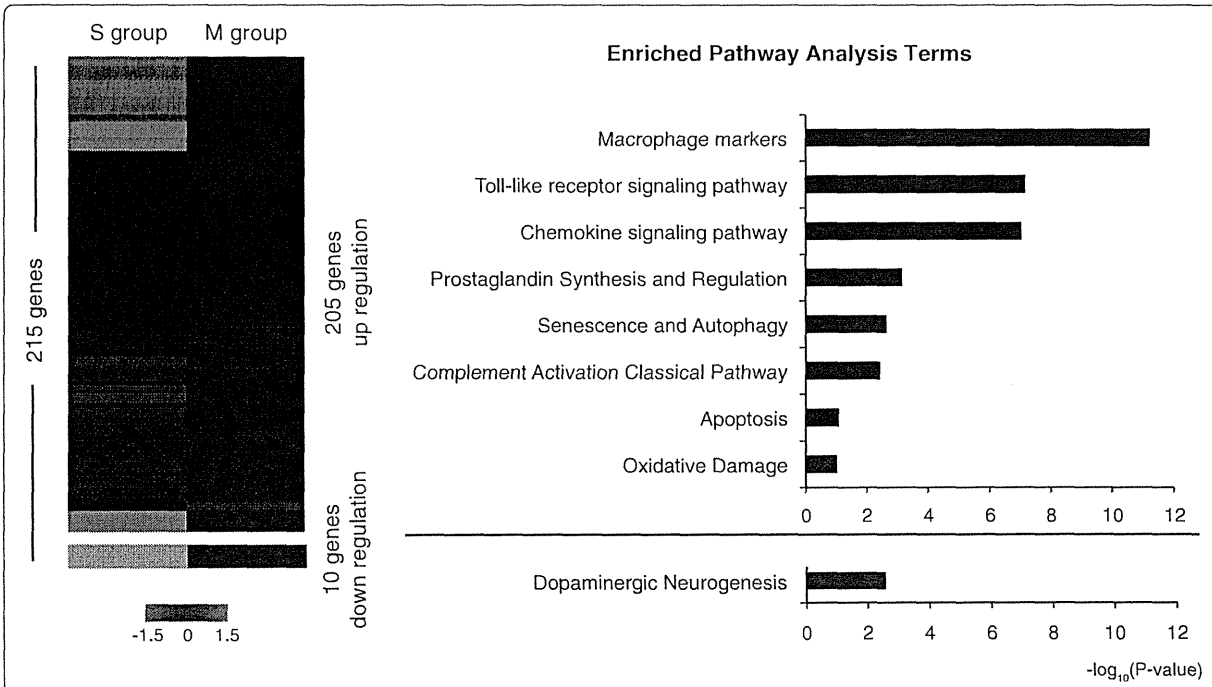


**Figure 2 Microarray analysis between severely and mildly compressed spinal cord in tip-toe walking Yoshimura *(twy)* mice.** Heat map (left panel) of 215 genes that differed significantly between the S and M groups ($n = 8$ mice per group). Upregulated genes in the S group are red, and downregulated genes are green. Scale is shown at the bottom. Pathway analysis terms (right panel) of the genes that differed between the S and M groups.

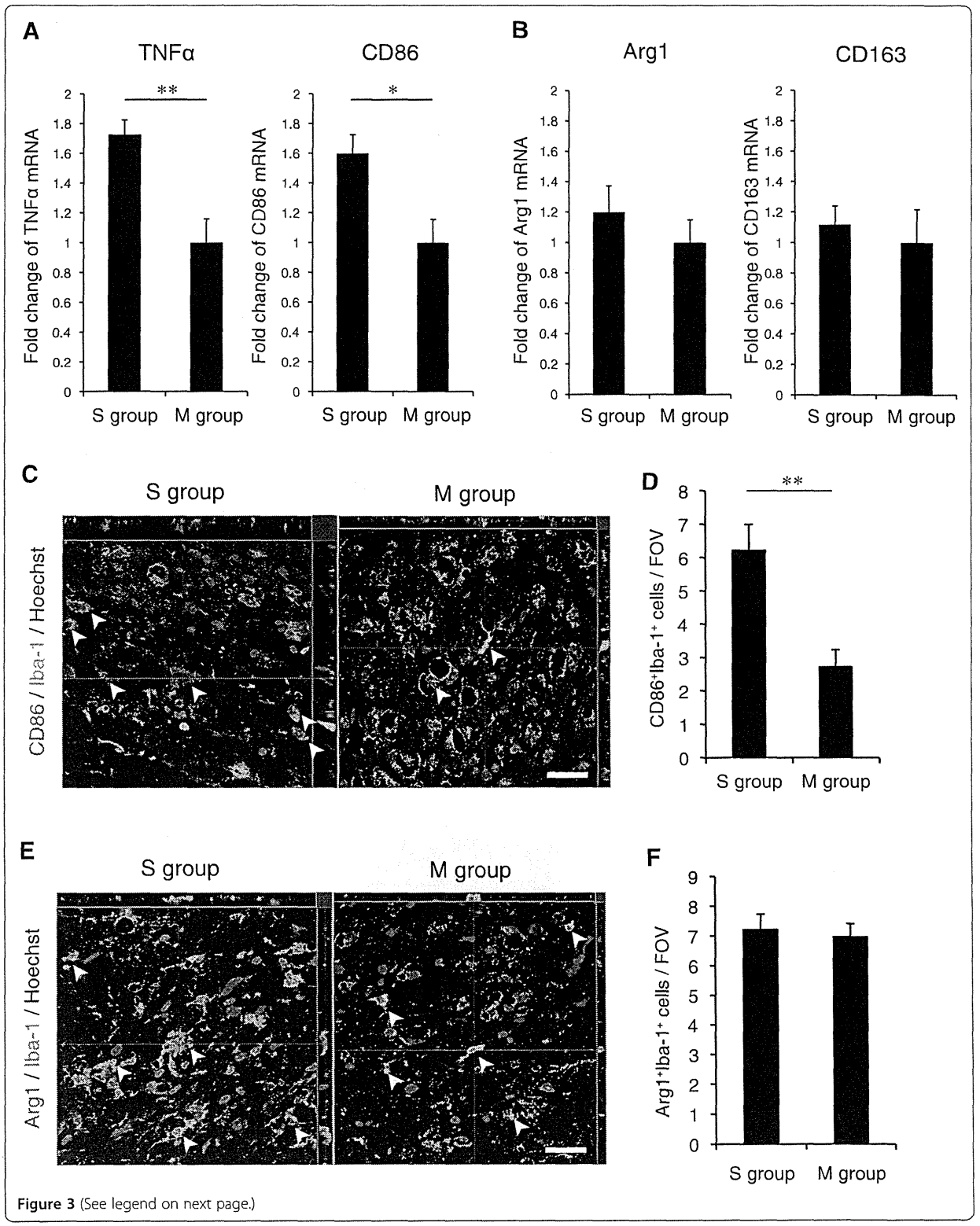


**Figure 3** (See legend on next page.)

(See figure on previous page.)
**Figure 3 M1 macrophages were the dominant activated macrophage phenotype in the severely compressed spinal cord. (A, B)** Fold change of the mRNAs for TNFα and CD86 (M1 macrophage markers), and for arginase1 and CD163 (M2 macrophage markers), determined by RT-PCR ($n = 4$ mice per group). $^{**}P < 0.01$, $^{*}P < 0.05$. **(C)** Representative magnified images of CD86/Iba-1 double-positive cells (arrowheads) in the S and M groups. Scale bar: 20 μm. **(D)** Quantitative analysis of the number of CD86/Iba-1 double-positive cells per field of view. $^{**}P < 0.01$. **(E)** Representative magnified image of arginase1 (Arg1)/Iba-1 double-positive cells in the S and M groups. Scale bar: 20 μm. **(F)** There was no significant difference in the Arg1/Iba-1 double-positive cells (arrowheads) between the S and M groups.

anti-Iba-1 (rabbit IgG, 1:200, Wako, Osaka, Japan), anti-CD86 (rat IgG, 1:200, Abcam, Cambridge, UK), anti-arginase-1 (goat IgG, 1:200, Santa Cruz Biotechnology, CA, USA), anti-Cyr61 (rabbit IgG, 1:200, Santa Cruz Biotechnology), anti-C1q (goat IgG, 1:200, Santa Cruz Biotechnology), and anti-PSD95 (mouse $IgG_{2a}$, 1:200, Millipore, MA, USA). The samples were examined with an inverted fluorescence microscope (BZ 9000; Keyence Co., Osaka, Japan) and an LSM 700 confocal laser-scanning microscope (Carl Zeiss, Munich, Germany). To quantify the HE-stained and C1q-immunostained sections, images obtained with the BZ9000 microscope were analyzed using Keyence Analysis Software (Keyence Co.). Constant threshold values were maintained for all the analyses. HE-stained images were taken at C2/3 (the lesion epicenter) in axial sections at × 20 magnification to measure the transverse area of the spinal cord. The CD86/Iba1-, Arg-1/Iba1-, and Cyr61-stained images were automatically captured at the compressed spinal cord area in axial sections at × 200 magnification, and the CD86/Iba1- and Arg-1/Iba1-positive cells per field of view in compressed spinal cords were quantified.

### Immuno-electron microscopy

Cryosections of severely compressed *twy* mouse spinal cord (20 μm) were incubated with 5% block ace (DS Pharma Biomedical., Osaka, Japan), 0.1% Saponin in 0.1 M phosphate buffer for 1 h. Sections were immunostained with a primary rabbit anti-Iba antibody (1:100 Wako) for 72 h, and nanogold-conjugated anti-rabbit secondary antibody (1:100 Invitrogen) for 24 h at 4°C. After fixation in 2.5% glutaraldehyde, the nanogold signals were enhanced with the HQ-Silver kit (Nanoprobes Inc.) for 10 minutes. The samples were post-fixed with 0.5% osmium tetroxide, dehydrated through ethanol, acetone, and QY1, and embedded in Epon. Ultrathin (80 nm) sagittal spinal cord sections were stained with uranyl acetate and lead citrate for 10 and 12 minutes, respectively. The sections were examined under a transmission electron microscope (JEOL model 1230) and photographed using a Digital Micrograph 3.3 (Gatan Inc., CA, USA).

### Statistical analysis

All values are presented as the mean ± standard error of the mean (s.e.m.). An unpaired two-tailed Student's *t*-test

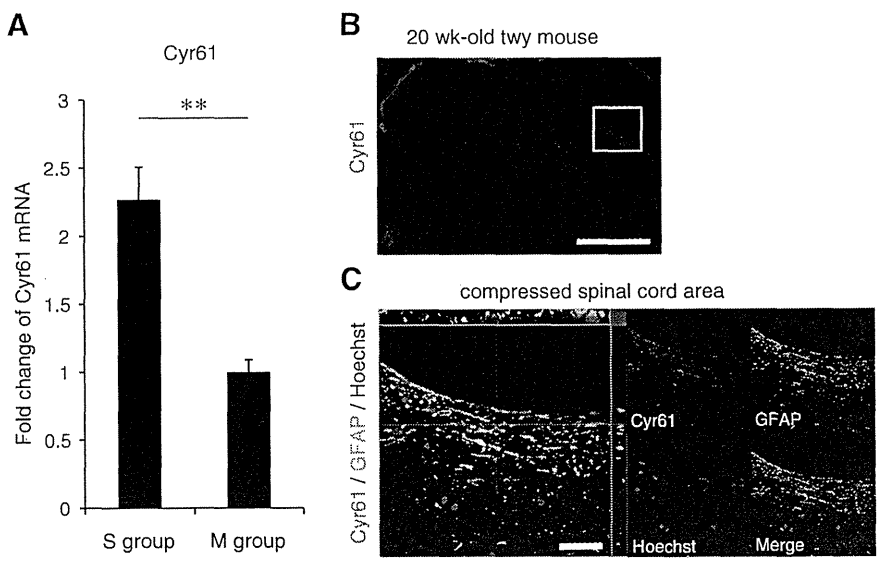


**Figure 4 Upregulation of Cyr61 in the severely compressed spinal cord. (A)** Fold change of the Cyr61 mRNA by RT-PCR ($n = 4$ mice per group). $^{**}P < 0.01$. **(B, C)** Cyr61-positive cells were located at the compressed area and highly colocalized with reactive astrocytes. Scale bar: 500 μm **(B)**, 20 μm **(C)**.

was used to determine the significance of differences in the behavioral, transcriptome, histological findings of each group. For all statistical analyses, significance was defined as $P$ <0.05. GraphPad Prism software (version 5.0d) was used for the analyses (GraphPad Software, Inc., CA, USA).

## Results

High-resolution MRI was performed when the mice were 6, 15, and 20 weeks old, as reported previously (Figure 1A) [10]. In the *twy* mice, spinal cord compression progressed at the C2/3 level due to ligamentous calcification. Twenty *twy* mice were divided into two groups according to the MRI findings: a severe compression group ($n$ = 8, S group) and a mild compression group ($n$ = 8, M group). The canal stenosis ratio was higher than 45% in the S group (average, 57.1%) and less than 25% in the M group (average, 11.1%) (Figure 1B and 1C). The other four *twy* mice were excluded from the analysis because they had moderate compression and could not be assigned to either group. The body weight was significantly lower in the S group than the M group (Figure 1D), and both the Rotarod treadmill latency and stride length were significantly decreased in the S group compared to the M group (Figure 1E and 1F). Consistent with the MRI findings, the spinal cord area of axial sections in the S group was significantly smaller than in the M group (Figure 1G and 1H).

To investigate the pathophysiology of the compressed spinal cord in detail, microarray analysis was performed for the S and M groups (Figure 2), as previously described [20]. This analysis revealed that the expression levels of 215 genes were significantly different between the S group and the M group; 205 genes showed increased expression in the S group, and 10 showed decreased expression. Pathway analysis revealed that the genes expressed at higher levels in the S group were enriched for terms related to macrophage markers, Toll-like receptor (TLR) signaling, and chemokine signaling, which regulate inflammation and gliosis in the injured spinal cord [21]. Furthermore, genes related to prostaglandin synthesis and regulation and to oxidative damage, which suggest ischemia of the compressed spinal cord [22], were upregulated in the S group. On the other hand, Neurogenin-2, which mainly regulates the differentiation of dopaminergic neurons ('dopaminergic neurogenesis') [23], was downregulated in the S group. Autophagy and apoptosis pathway components were also upregulated in the S group, consistent with previous reports [11,24].

To evaluate the macrophage phenotype in the two groups, cervical spinal cord samples were subjected to

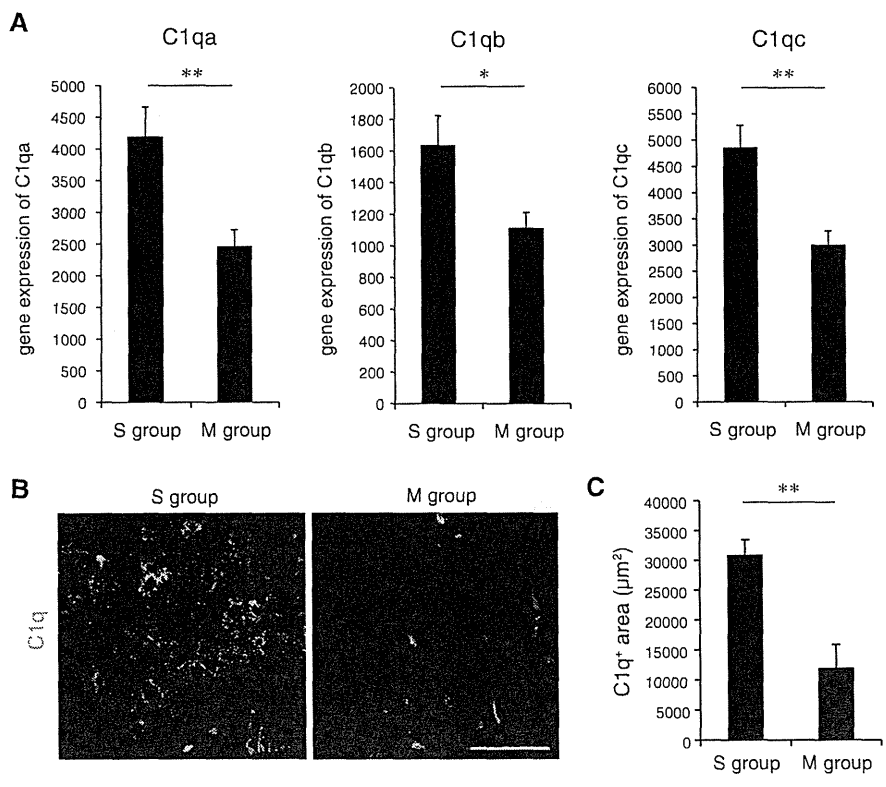


**Figure 5 Upregulation of the complement classical pathway in the severely compressed spinal cord. (A)** Expression of C1qa, C1qb, and C1qc mRNAs determined by microarray analysis ($n$ = 8 mice per group). **$P$ <0.01, *$P$ <0.05. **(B)** Representative images of the C1q-positive area in the S and M groups. Scale bar: 50 μm. **(C)** Quantitative analysis of the C1q-positive area in the S and M groups ($n$ = 4 mice per group). **$P$ <0.01.

RT-PCR and histological analyses. The mRNAs encoding TNFα and CD86, markers of the M1 phenotype, were significantly increased in the S group compared to the M group (Figure 3A), whereas there was no significant difference in the mRNAs for arginase1 or CD163, which indicate the M2 phenotype (Figure 3B). Histological analyses also showed that the number of double-positive cells for CD86 and Iba1, a microglia/macrophage marker, per field of view (FOV) (1 FOV = 100 × 100 $\mu m^2$) was significantly higher in the S than in the M group (Figure 3C and 3D), whereas there was no significant difference in the number of Iba1/arginase1-positive cells (Figure 3E and 3F).

M1 macrophages are recruited by chemotaxis in response to cysteine-rich protein 61 (Cyr61) [25], which is induced by mechanical stress [26,27]. We therefore examined the gene expression of Cyr61 in the cervical spinal cord of the S and M groups. Cyr61 was significantly upregulated in the S compared to the M group (Figure 4A), and Cyr61-positive cells were located at the compressed area and colocalized extensively with reactive astrocytes (Figure 4B and 4C).

To examine the mechanism of the neurodegeneration associated with inflammation in the chronically compressed spinal cord, we focused on the complement activation classical pathway (Figure 2). Previous reports suggested that at the early stage of neurodegenerative diseases and normal aging, C1q plays an important role in the pathophysiological process that leads to synapse loss and ultimately to neuronal death [28-31]. Our microarray analysis showed that the C1qa, C1qb, and C1qc expression levels were significantly higher in the S than the M group (Figure 5A). The area of punctate C1q staining was also significantly greater in the S than the M group (Figure 5B and 5C). Interestingly, many of the C1q-positive puncta that were close to microglia/macrophages in the compressed spinal cord were associated with synaptic puncta identified by double immunostaining with synaptic markers such as PSD-95 (Figure 6A). To confirm

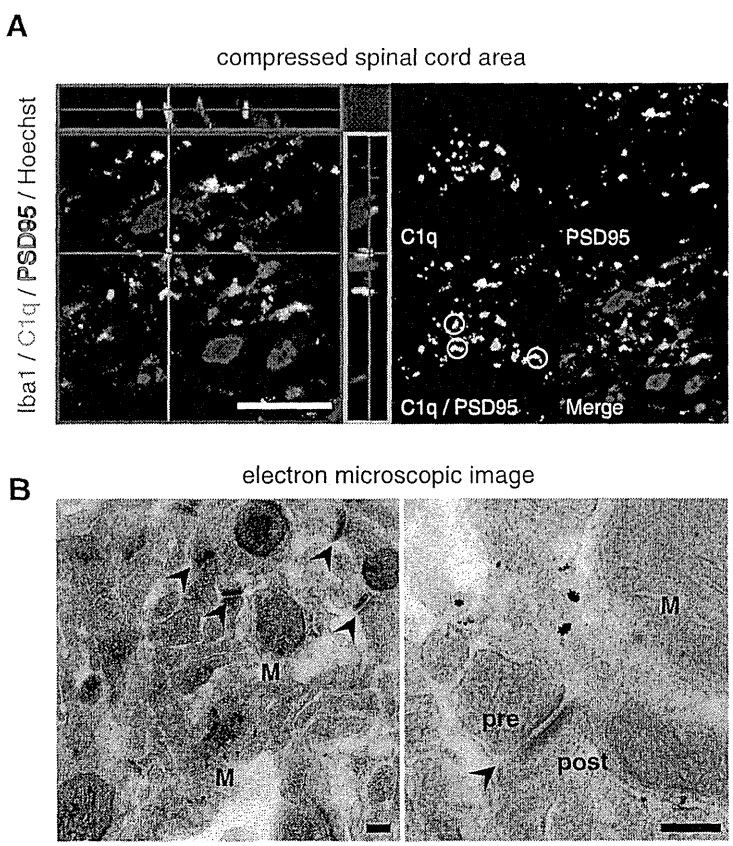


**Figure 6 Classical complement activation pathway-mediated synapse elimination in the severely compressed spinal cord. (A)** Representative magnified image of the Iba-1/C1q/PSD95 triple-positive area in the compressed spinal cord. Many C1q-positive puncta were colocalized with the postsynaptic protein PSD95 (several examples are circled). Scale bar: 10 μm. **(B)** Electron microscopic image of the compressed spinal cord, showing extensive contact between presynaptic/postsynaptic elements and activated microglia/macrophage processes. Scale bar: 0.2 μm. (arrowhead; synapse, pre; presynapse, post; postsynapse, M; microglia/macrophage).